REGIONALIZATION OF WIND-SPEED DATA TO ANALYSE TREE-LINE WIND CONDITIONS IN THE EASTERN ANDES OF SOUTHERN ECUADOR

Julia Wagemann, Boris Thies, Rütger Rollenbeck, Thorsten Peters and Jörg Bendix

With 8 figures, 4 tables and 1 photo
Received 3 November 2014 · Accepted 25 January 2015

Summary: This paper presents a method to extrapolate wind-speed data and to calculate wind-speed and dynamic pressure maps for the complex topography of a mountain rainforest area in the tropical Andes of southeastern Ecuador. The spatial differentiation of dynamic wind pressure in this area is claimed to be a major determinant of the altitude of the tree-line ecotone and to affect the tree line's physiognomy. The paper presents a hybrid method encompassing statistical data analysis using the Weibull distribution and a digital terrain analysis, taking topographical shelter effects into account. The method is used to derive mean and maximum wind-speed and dynamic pressure maps to reveal whether the tree-line ecotone is influenced by direct wind effects. On average, the tree-line ecotone on the eastern slopes shows a clear average depression of ~50 m. These slopes are affected by higher dynamic wind stress, so have a more disturbed canopy. These altered vegetation structures may be caused mainly by direct wind effects and to a smaller extent by indirect effects, such as high humidity.

Zusammenfassung: Es wurde eine Methode entwickelt, um räumliche Windgeschwindigkeits- sowie Staudruckkarten für ein topographisch diverses Gebiet in den tropischen Anden Südecuadors zu generieren. Die räumliche Variabilität des dynamischen Staudrucks beeinflusst entscheidend die Höhenposition und Physiognomie des lokalen Waldgrenzökotons im Studiengebiet. Eine Hybridmethode aus statistischer Daten- und digitaler Geländemodellanalyse, um mittlere und maximale Windgeschwindigkeits- sowie Staudruckkarten zu generieren, wird präsentiert. Mithilfe der Weibull-Verteilung werden dabei die Winddaten statistisch beschrieben und Höhen- sowie Topographieeffekte werden bei der Interpolation mit berücksichtigt. Die generierten Karten werden anschließend für weitere Baumgrenzökotonuntersuchungen herangezogen. Hierbei wird hauptsächlich untersucht, ob die Herabsetzung des Baumgrenzökotons im Studiengebiet auf den Einfluss direkten Windstresses zurückzuführen ist. Im Durchschnitt ist das Baumgrenzökoton der östlichen Hänge im Studiengebiet um ~50 m herabgesetzt. Osthänge werden stärker durch dynamischen Windstress beeinflusst. Die daraus resultierenden Veränderungen der Vegetationsstruktur des Baumgrenzökotons sind größtenteils auf direkte Windeffekte und zu einem kleineren Teil auf indirekte Effekte, wie z.B einer erhöhten Feuchtigkeit, zurückzuführen.

Keywords: Statistical wind-speed analysis, digital terrain analysis, upper tree line, Weibull distribution, dynamic pressure, Southern Ecuador

1 Introduction

Wind in complex terrain has a high spatio-temporal variability and is influenced by the synoptic conditions, topography and land cover. In complex topography, local mountain breezes interact with larger-scale circulation patterns (Bendix et al. 2008; Bendix 2004). Strong winds and their resulting dynamic pressure (the forces they produce) are able to alter vegetation structures and may have a major influence on the predominant tree line and its position. Early work in the European Alps pointed out adverse wind effects at higher slope positions exposed to strong synoptic winds, lowering the tree line (in the so-called "Kampfzone") because wind was proven to clearly reduce the growth height, particularly of young trees. Furthermore, investigations in the Alps and at Mount Fuji, Japan, show that strong winds cause a streaky shape of the tree-line ecotone and tree deformations (e.g. Aulitzky 1961; Aulitzky 1962a; Turner 1971; Yoshimura 1971). More recently, a review by Holtmeier and Broll (2010) stressed that greater attention should be given to the varying wind effects impacting the altitude of the tree-line ecotone, particularly with respect to possible impacts of global climate change on tree-line position.

On a global scale, Körner (1998) and Körner and Paulsen (2004) emphasize the dominating effect of temperature to explain the position of potential natural tree lines. At a landscape and local scale, however, temperature as the key climatic factor is mostly recognized to be blurred by a combination of multiple interacting factors, such as topography,

DOI: 10.3112/erdkunde.2015.01.01 ISSN 0014-0015 http://www.erdkunde.uni-bonn.de

moisture availability, solar radiation or even strong winds (Holtmeier 2009; Holtmeier and Broll 2010; Malansson et al. 2011).

Peters (2009) investigated a local tree-line depression (see Photo 1) on the windward side of a crest in the Cordillera Real, in the eastern Andes of southern Ecuador (the same area as the current paper). This study revealed that the negative effects of high wind speeds are more important especially at the local scale. For the Ecuadorian Andes, the thermally limited tree line is normally at around 4,000 m a.s.l. (Bendix and Rafiqpoor 2001). However, in the Andes of southern Ecuador, it is clearly depressed to around 2,900–3,200 m a.s.l. (Richter et al. 2008; Göttlicher et al. 2009; Peters 2009).

Methodological uncertainties when comparing tree-line position to potential environmental drivers often result from a lack of meteorological data and, in particular, a lack of spatially explicit data in remote mountainous areas. Spatial wind maps are needed to investigate the direct and indirect effects of wind exposure on the elevation of the tree-line ecotone; these can then be blended with spatial data of the tree-line position taken from an analysis of satellite data. So far, several investigations to interpolate wind speed have used common spatial interpolation methods and geostatistics (Luo et al. 2008; Etienne et al. 2010; Palomino and Martin 1994; Xia et al. 2000). But these methods give little consideration to topographical and altitudinal effects, so are less useful in complex terrain. To solve these shortcomings, Ryan (1977) and Wörlen et al. (1999) suggested considering the sheltering effects of the topography when extrapolating wind speed in complex terrain. The current study presents a hybrid method of statistical data and digital terrain analysis to generate mean and maximum wind-speed maps for a topographically complex area in the Cordillera Real of southern Ecuador, a hotspot of biodiversity (Beck et al. 2008; Bendix and Beck 2009). While the wind field and its effects on the study area have already been analysed based on station data (e.g. Bendix et al. 2008), the regionalization of wind-speed data and an analysis of its potential effect on the regional tree-line position was still lacking.

The current paper has two aims. First, it demonstrates an approach to generate regionalized wind-speed maps incorporating altitudinal and topographical effects. These maps serve to calculate dynamic pressure maps of the study area. Second, the dynamic pressure maps are blended with the local tree-line ecotone derived from a satellite-based land-cover classification to reveal the potential influence of dynamic pressure as a direct wind effect on the position of the tree-line ecotone. Indirect effects of wind exposure will also be discussed.

Photo 1: Local timberline ecotone at El Tiro. The photo shows the crest line running from north to south. Especially the eastern flanks (left) and narrow ridges are covered by Páramo vegetation, whereas the western flanks (right) are shrouded by dense forest up to the highest crests. (Photo: Thorsten Peters)

2 Study area

The core of the study area is the Reserva Biológica San Francisco (RBSF) (3° 58' S, 79° 04' W) around the ECSF (Estación Científica San Francisco) research station (Fig. 1), in the Cordillera Real of the eastern Andes of southern Ecuador. It is the main study area of an interdisciplinary ecological research programme and has been the subject of several detailed ecological and climatic studies since 1997 (e.g. Beck et al. 2008; Bendix and Beck 2009; Fries et al. 2012 and many others). The wider study area includes the main eastern Andean cordillera chain encompassing the Podocarpus National Park. The general climate of the study area is characterized by distinct horizontal and vertical gradients, for example a strong difference in annual rainfall in a small horizontal distance (~20 km), ranging from about 900 mm for Loja, the provincial capital in the west, to ~6,000 mm at the highest point in the core study area, the Cerro del Consuelo (Cerro) in the east (e.g. Rollenbeck et al. 2011). The area's near-surface flow field (2 m above ground level) is influenced by a complex interaction between different circulation regimes. In the upper parts, the tropospheric easterlies predominate throughout the year (>90% in JJA), with an increase of westerly wind directions in the southern hemisphere summer (up to ~50% in November) (Bendix et al. 2008; Rollenbeck and Bendix 2011). In the valleys, the wind field is modi-

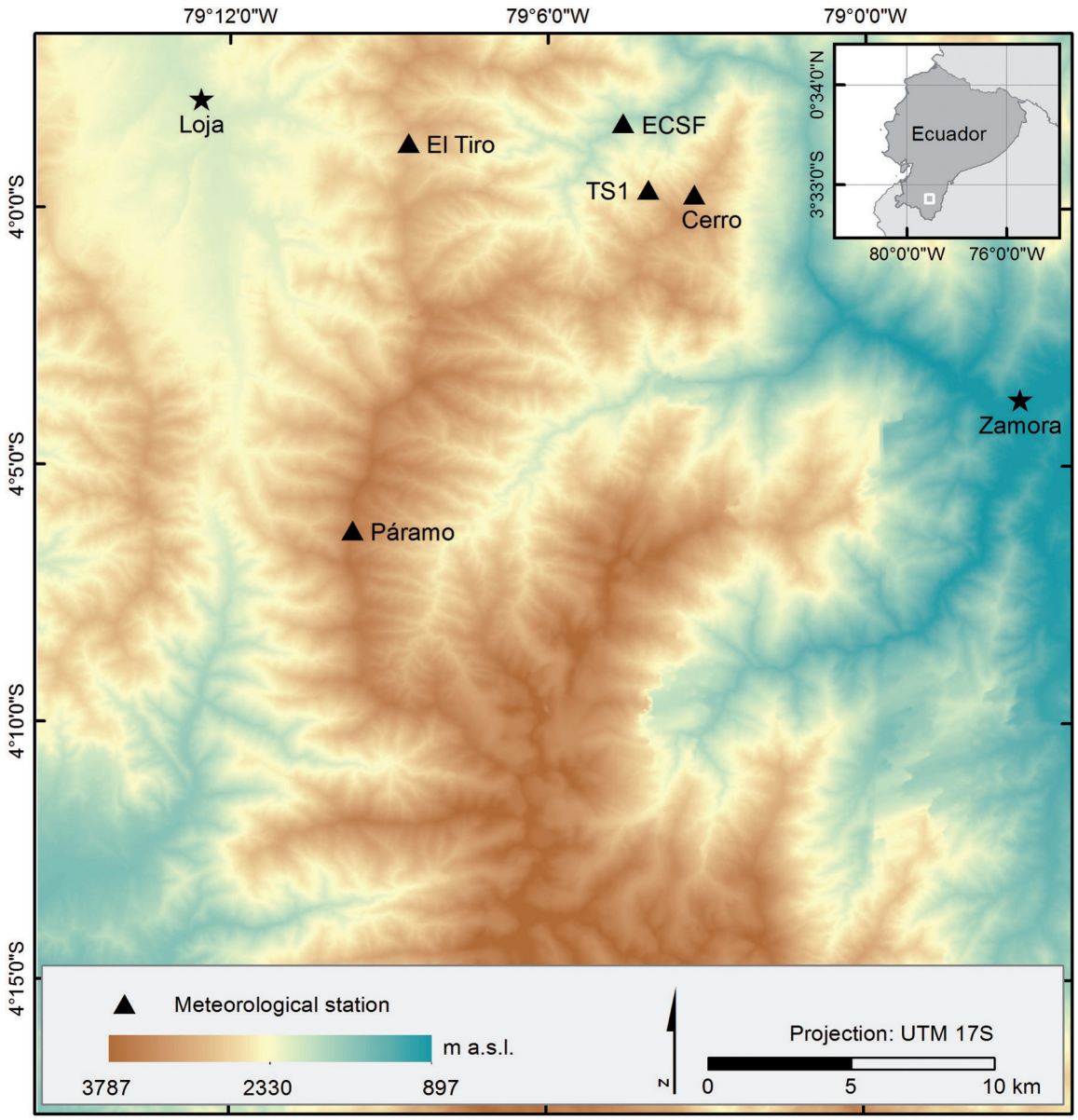

Fig. 1: Study area and location of meteorological stations

fied by diurnal breeze systems; these generally have lower wind speeds (Bendix et al. 2008; Bendix et al. 2009; Trachte et al. 2010).

3 Data and Methods

The current study is based on hourly wind-speed data of five fully automatic meteorological stations (Tab. 1) operated in the scope of the ecological research programme, and a high-resolution digital elevation model (DEM, Fig. 1). It uses hourly measured wind-speed and wind-direction data at 2 m above ground level for a period of eight years (16 May 1999 to 21 October 2006). All the statistical analyses presented here were conducted for the whole data set of each meteorological station and for eight wind-direction classes (N, NE, E, SE, S, SW, W, NW). Additionally, wind-speed data from the official INAMHI (Instituto Nacional de Meteorología e Hidrología) station at Zamora (Fig. 1) in the foothills of the eastern Andes (970 m a.s.l., lat: 4° 05' S, long: 78° 57' W) is used. The digital elevation model used was processed in 2004 by triangulation of stereo aerial photos recorded by the

Tab. 1: Meteorological stations in the study area

Station no.	Name	Latitude	Longitude	Altitude (m)
1	Cerro	3° 59' 44" S	79° 03' 14" W	2,930
2	ECSF	3° 58' 21" S	79° 04' 35" W	1,957
3	El Tiro	3° 58' 45" S	79° 08' 38" W	2,825
4	Páramo	4° 06' 16" S	79° 07' 63" W	3,400
5	TS1	3° 59' 39" S	79° 04' 06" W	2,669

research programme (for the method refer to JORDAN et al. 2005), resulting in a grid resolution of 10 m.

The regionalization of wind speed and wind dynamic pressure was conducted in four main steps (Fig. 2):

- a statistical analysis of the wind-speed data using the Weibull density function;
- the regionalization of the wind speed by applying altitudinal gradients of wind speed and a terrain sheltering factor derived from a DEM;
- the validation of regionalized and independently measured wind-speed data by means of a regression analysis and
- the calculation of dynamic pressure from the tropical standard atmosphere and the derived maps of wind speed

3.1 Statistical analysis of wind-speed data

It is crucial for various ecological studies to know about the mean and maximum wind speed at a certain location. However, it is a challenge to generate an accurate statistical model of wind speed including representative average and maximum values. This is because the wind speed may change in seconds from gust to calm, and is particularly variable in complex terrain (WEISSER 2003). From a statistical point of view, the frequency distribution of wind-speed data is generally derived from wind-speed classes of 0.5 m s^{-1} or 1 m s^{-1}. The Weibull density function is the most common approach applied to wind-speed data because of its great flexibility and simplicity as well as its good fit to experimental data (LUN and LAM 2000; WEISSER 2003).

The three-parameter Weibull distribution is mathematically expressed as follows:

$$f_x(x / A, B, C) = C/B * [(x\text{-}A) / B]^{C-1} * exp [- ((x\text{-}A) / B)^C] \quad (1)$$

where f_x (x/A,B,C) is the probability of observing a wind speed x ($x \geq A$), A is the Weibull location parameter, B is the Weibull scale parameter, and C is the dimensionless Weibull shape parameter (RINNE 2009).

There are several ways to fit the Weibull distribution to specific wind-speed records by deriving the three parameters A (location), B (scale) and C (shape). The two most common approaches for wind-speed data examination are the ordinary least square (OLS) and the maximum likelihood estimation (MLE) (WILKS 2008). In this study, an approach developed by PENNYPACKER et al. (1980) was used which allows for both procedures, OLS and MLE. First the approach tries to estimate B and C using MLE. If wind-speed data do not fit a Weibull maximum-likelihood probability density function, the approach uses OLS, where A ($A < x$) is used to normalize the data.

Once the three parameters of the Weibull distribution are estimated, the frequency distribution (Eq. 1) was calculated. The goodness of fit of the derived distribution is graphically assessed by plotting the Weibull probability density curve together with the frequency distribution of the sample data for each meteorological station and wind-direction class. Instead of using the average and maximum values of wind speed, the 50th (P50) and 95th percentile (P95) values of the calculated Weibull frequency distribution are used (WILKS 2008). In the following sections we refer to the terms mean and maximum to describe the 50th and 95th percentiles respectively.

3.2 Regionalization of wind speed

The meteorological station Páramo (Fig. 1, Tab. 1) with the highest elevation was chosen as the reference station for the regionalization approach as it best represents the topographically

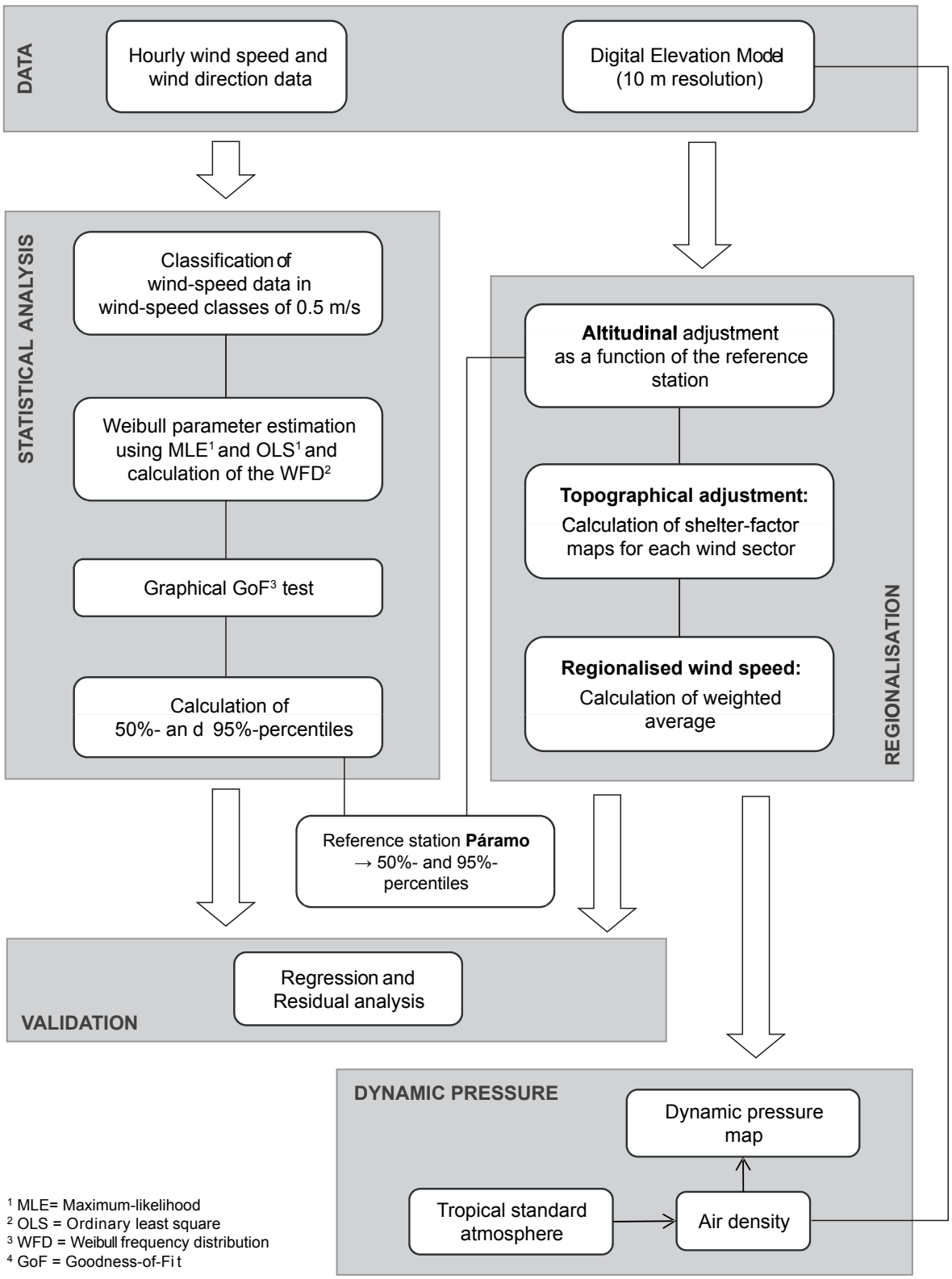

Fig. 2: Work flow of the study

undisturbed synoptic wind regime (EMCK 2008). Its P50 and P95 values were used to calculate maps of average and maximum wind speeds. For the regionalization, information about altitudinal and topographical effects influencing the wind speed at a specific 10 m grid cell are retrieved by digital terrain analysis, where two different analyses were conducted: (i) an altitudinal and (ii) a topographical adjustment.

(i) Wind speed increases with altitude. It is assumed that wind speeds at the reference station Páramo are the highest. Due to the altitudinal gradient, a decrease in wind speeds at lower altitudes is expected. Mean wind speeds at five different altitudes (data from the stations Páramo, El Tiro and Cerro, as well as from the cities Loja and Zamora), between 970 m and 3,400 m, were used to approximate the relationship between wind speed and altitude. Their relative decrease of wind speed as a function of the reference station was calculated. The resulting equation was applied to the Digital Elevation Model to create a reduction-factor map. This map shows the decline or increase of wind speed due to altitude, relative to the reference station Páramo.

(ii) Wind in mountainous areas is influenced by a multitude of factors which have been included in various mathematical models. RYAN (1977) conducted a study based on the assumption that different factors such as topography, sea and land breezes, and slope wind, have an additive vector character for the resulting mountain wind. WINSTRAL and MARKS (2002) developed another approach to quantify wind shelter when they simulated wind fields and snow redistribution by applying terrain-based parameters. They introduced the maximum upwind slope parameter *Sx* (in degrees), which is a measure of topographic shelter or exposure relative to a particular wind direction. The *Sx* algorithm is defined as follows:

$$Sx_{A,dmax}(x_i,y_i) = max(arctan\ \{[z*(x_v,y_v) - z*(x_i,y_i)] / sqrt[(x_v - x_i)^2 + (y_v - y_i)^2]\} \quad (2)$$

where *A* indicates the wind direction, *dmax* is the lateral extent of the search, *z* is the altitude (m a.s.l.) of a pixel, (x_i, y_i) are the coordinates of the cell searched by the algorithm, and (x_v, y_v) are all cell coordinates along the line segment defined by (x_i, y_i), *A*, and *dmax* (WINSTRAL and MARKS 2002).

The shelter factor (*Sx*) corresponds to that factor by which the wind speed is decreased. In the current study we apply the method of WINSTRAL and MARKS (2002) to calculate shelter-factor maps for the eight wind sectors, with the digital elevation model as the basis for applying the sheltering-factor-algorithm (Eq. 2).

The regionalized mean and maximum wind-speed maps were calculated in two steps. The first step was to multiply the mean and maximum values for the Páramo station (50th and 95th percentile from Weilbull distribution) with the relative decrease of wind speed as a function of height (derived from step (i)) for each DEM pixel in the study area. In a second step, the adjusted wind speed at every grid point was multiplied by (1 minus the shelter factor at every grid point for each of the eight wind sectors) resulting in the final topographically adjusted mean and maximum wind-speed maps for each of the eight wind sectors. An overall mean and maximum wind-speed map for the study area integrated over all wind sectors was finally derived from the weighted mean of the eight regionalized wind-speed maps. For this, each wind sector map was multiplied by a weighting factor based on the frequency of wind observations per wind-sector class at the reference station.

3.3 Validation

To validate the quality of the interpolated regionalized mean and maximum wind-speed maps, the statistically analysed wind-speed values (50th and 95th percentiles of the Weibull distribution) of the meteorological stations El Tiro, Cerro and ECSF were compared with the extracted pixel values of the regionalized wind-speed maps at the respective station locations. The validation procedure encompasses four regression models: (i) two for mean and maximum wind speeds at the three stations Cerro, ECSF and El Tiro, (ii) another two for mean and maximum wind speeds excluding the station El Tiro because this station caused insignificant validation results due to channelling effects caused by its specific location. The GPS coordinates for station data, especially in mountainous areas, and/or the topographical data may be inaccurate by tens of meters. Therefore the arithmetic mean of extracted wind speeds of a 3x3-pixel window around the meteorological station was used for validation.

3.4 Analysis of wind dynamic pressure at the tree-line ecotone

With help of the regionalized wind-speed maps and the digital elevation model, the dynamic wind pressure was calculated for every grid cell as follows:

$$q_{ref} = \rho\ (v_{ref})^2 / 2 \quad (3)$$

where q_{ref} is the dynamic pressure on an area of 1 m^2 (N m^{-2}), ρ is the air density (kg m^{-3}) and v_{ref} the regionalized wind speed (m s^{-1}). The map of the standard air density ρ was calculated as a function of terrain elevation taken from the DEM by applying an exponential fit ($r^2 = 0.9997$) derived from tabulated values of the tropical standard atmosphere:

$$\rho = 1.1854 * exp[-0.0001 * z] \quad (4)$$

where z is the terrain altitude (m a.s.l.) at a grid cell, taken from the DEM.

The mean and maximum dynamic pressure (Eq. 3) of the study area was calculated based on the air-density map (Eq. 4) and the regionalized mean and maximum wind-speed maps.

The dynamic pressure maps made it possible to (i) investigate the wind situation at the tree-line ecotone and (ii) analyse whether the wind pressure had a direct effect on the altitude of the tree line. The spatial distribution of the study area's tree-line ecotone was obtained with the help of an existing land-cover classification (for the method refer to Göttlicher et al. 2009), which distinguished between 15 vegetation classes after Homeier et al. (2008). For the GIS analysis, the land-cover classes Subpáramo and Páramo were extracted; their boundaries define the position of the tree-line ecotone. To analyse the wind conditions at the tree line, the extracted tree-line ecotone was intersected with the mean and the maximum dynamic pressure maps and classified into eight wind sectors. The results were further classified into six dynamic pressure classes; mean dynamic pressure in six classes with a width of 5 N m^{-2} and maximum dynamic pressure in six classes with a width of 20 N m^{-2}. Each set of dynamic pressure classes thus reflect two low-level, two mid-level and two high-level dynamic pressure classes. Further, the altitudinal difference of the tree-line position on the eastern and western slopes, and the actual mean height of easterly (NE, E, SE) and westerly (SW, W, NW) pixel expositions of the altitudinal distribution of the tree line were quantified and the difference between the easterly and westerly pixel expositions was calculated. This showed whether the wind pressure had a direct influence on the tree line's altitude and physiognomy.

4 Results

4.1 General wind characteristics at the meteorological stations

The high variability in space and time of wind and the existence of different local and regional wind systems in the investigation area was confirmed by wind-rose diagrams for the five meteorological stations (Fig. 3). The three stations Cerro (2,930 m), El Tiro (2,825 m) and Páramo (3,400 m) possess the highest average wind speeds, ranging from fresh breezes (Beaufort scale [BS] 5) to near gales (BS 7). More than half the wind-speed data showed wind directions from northeast, east and southeast at these sites, so are dominated by the synoptic wind conditions that prevail in the study area (Rollenbeck and Bendix 2011). ECSF (1,957 m) and TS1 (2,669 m) show a dominance of light breezes (BS 2) and scattering. ECSF features the characteristics of a typical mountain-valley wind system. An up-valley wind occurs during the day, down-valley during the night. Therefore ECSF´s wind speeds are dominated by wind blowing from the southwest and northeast. In contrast, wind speeds at TS1 are strongly scattered and have no prevailing direction. In general, mean wind speeds at the high-level stations are in the range of moderate (BS 4) to fresh breezes (BS 5) and are much lower at low-level stations, where the mean wind speeds are just light airs (BS 1).

4.2 Statistical analysis of station wind data

For each station the three parameters of the Weibull distribution function for the entire data set as well as the eight wind sectors were extracted (Tab. 2). Some data sets cannot be described by a maximum-likelihood probability density function. For most of the data sets examined in this study, the OLS estimates were more robust and had a better fit than the parameters estimated by MLE. In some cases, however, only the MLE estimates were able to statistically describe the data set (Tab. 2, entries marked with an asterisk).

To test the suitability of the Weibull distribution to describe the wind-speed distribution at the meteorological station, a graphical assessment of the

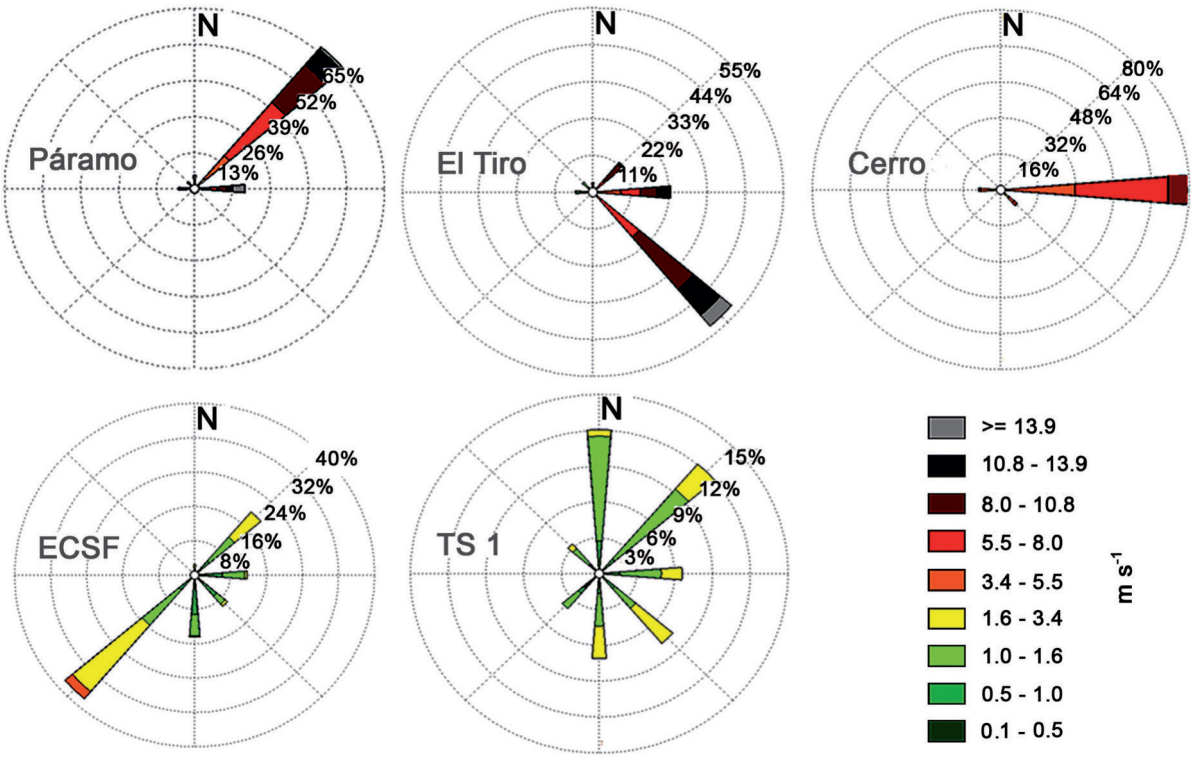

Fig. 3: Wind roses (m s^{-1}) for each of the five meteorological stations 1999–2006 (Wind-speed classes of the wind roses were classified referring to the Beaufort wind scale)

Tab. 2: Calculated Weibull parameters of the five meteorological stations

		ALL	N	NE	E	SE	S	SW	W	NW
	Location A	0*	0*	0*	0.82	1.00	-0.14	0.20	0.48	0.82
El Tiro	Shape B	19.55*	15.55*	17.59*	16.81	22.20	3.13	2.36	2.14	2.20
	Scale C	1.76*	1.17*	1.942*	2.13	3.10	2.52	2.86	2.59	2.34
	Location A	-2.15	0*	1.00	-2.56	1.00	1.00	1.00	0.33	1.00
Páramo	Shape B	20.32	21.70*	18.53	23.34	5.93	6.82	5.64	9.34	5.48
	Scale C	2.17	1.60*	2.26	2.34	1.45	1.28	1.28	1.77	1.62
	Location A	0.54	0.27	0.71	0.35	0.40	0.39	1.00	0.57	-0.17
ECSF	Shape B	2.89	3.15	3.06	3.18	2.29	2.13	3.08	2.52	3.51
	Scale C	1.88	2.44	2.14	1.85	1.67	2.32	1.67	1.69	3.03
	Location A	n.a	n.a	n.a	n.a	n.a	n.a	n.a	n.a	n.a
TS1	Shape B	n.a	n.a	n.a	n.a	n.a	n.a	n.a	n.a	n.a
	Scale C	n.a	n.a	n.a	n.a	n.a	n.a	n.a	n.a	n.a
	Location A	-23.19	0.79	0.92	-7.95	-3.66	0.99	0.32	-5.12	-1.82
Cerro	Shape B	36.98	0.50	0.35	22.16	13.01	0.50	3.71	16.65	11.50
	Scale C	7.89	1.00	1.00	5.36	2.54	1.00	1.00	2.34	1.45

Note: values indicated with * are MLE estimates; all other parameter are OLS estimates

goodness-of-fit (GoF) was conducted (see a selection of GoF results in figure 4). Wind speeds at the station Páramo (a) and ECSF (b) could be properly described by the Weibull distribution. At El Tiro (d), however, the wind-speed frequency distribution is partly bimodal, which results in limited GoF-test results, even if the parameters could be properly derived (Tab. 2). The fit lowers the 50th percentile by 0.69 m s^{-1} (8.39 m s^{-1} to 7.7 m s^{-1}) and raises the 95th percentile by 2.59 m s^{-1} (15.5 m s^{-1} to 18.1 m s^{-1}). The graphical GoF results for the wind direction north at station Cerro (c) reveal, for example, that it was not possible in every case to achieve a good fit of the measured station data to the Weibull PDF (probability density function) curve. Besides the northerlies, the wind directions northeast and south at station Cerro could not be fitted properly, even if the distribution parameters could be calculated. The reason might be slight channelling effects due to the topographic location of the meteorological station on a crest running north-south surrounded by higher peaks. The Weibull parameters were used to calculate the Weibull PDF in order to extract the 50th and 95th percentiles (Tab. 3).

For the high-altitude stations El Tiro and Páramo, as well as for the low-altitude station ECSF, the 50th and 95th percentiles of the entire data set and of the eight individual wind directions were determined. For the station Cerro, only the mean and maximum percentiles for the entire data set, the east and the northwest directions could be extracted. The data sets of the other wind directions could not be fitted properly to a Weibull distribution function. The same constraints of the Weibull distribution were apparent at station TS1. This station is characterized by an exceptionally high rate (41%) of wind speeds lower than 1 m s^{-1}, which strongly limits the adjustment of a Weibull PDF curve. No mean and maximum percentiles could be determined for this station, which eventually led to its exclusion

Tab. 3: Results of statistical wind data analysis (all wind sectors) for five meteorological stations (wind speed is given in m s^{-1})

	El Tiro	Páramo	ECSF	TS1	Cerro
Mean wind speed	8.0	7.8	1.3	0.6	5.6
Calms in %	0	0	0	0	0
50% percentile	7.7	7.4	1.2	n.a	6
95% percentile	18.1	16.4	2.5	n.a	10.1

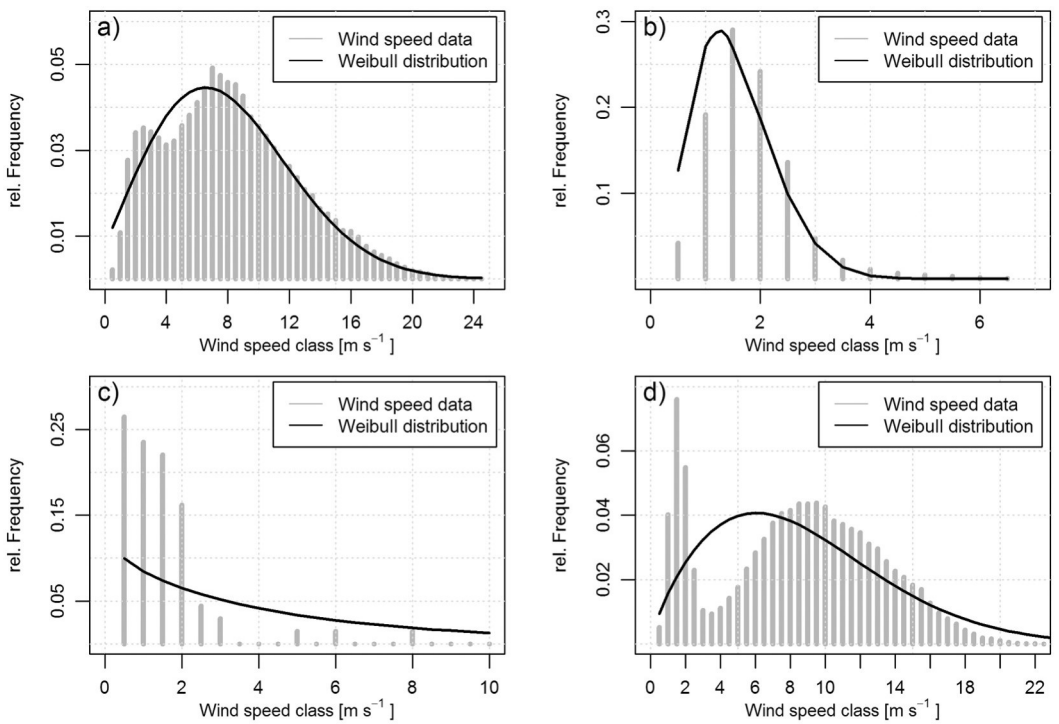

Fig. 4: Demonstrative results of the graphical goodness-of-fit tests for the meteorological stations (a) Páramo*, (b) ECSF*, (c) Cerro and (d) El Tiro* (* refer to all wind sectors; ** refer only to northerlies)**

from all further analyses. All other stations where percentiles could be extracted properly are used in the validation procedure.

4.3 Wind-speed maps and their validation

Figure 5 shows the derived mean and maximum wind-speed maps. Mean wind speeds ranged from 0.1 m s^{-1} to 8.6 m s^{-1}, whereas maximum wind speeds rose to 17 m s^{-1}.

It is obvious that the crest areas of the cordillera chains experience the highest wind-speed values, while the protected valleys, mainly on the eastern slopes, are mostly sheltered from the influence of the strong synoptic winds. The more open basin of Loja is characterized by moderate mean and maximum wind speeds because it is less protected by the surrounding topography.

The regression models for validating the entire wind-speed maps, including the meteorological stations Cerro, ECSF and El Tiro, attained significant p-values, though the values for the adjusted R^2 show that only a small percentage of the variance could be explained (Tab. 4, left). As expected, if El Tiro was included, some outliers were notable and reduced the quality of the regression models. Excluding El Tiro improved the regression models significantly (Tab. 4, right). The regression model of the mean wind speed no longer incorporated an obvious outlier, resulting in a highly significant p-value. At maximum wind speed, only the strongly underestimated northwesterlies at station Cerro remained as an outlier.

4.4 Dynamic pressure maps and the tree line

The resulting mean and maximum dynamic pressure maps are shown in Figure 6. The highest dynamic pressures occurred mainly at the crest regions. Vegetation around the crest region and east-facing slopes has to withstand dynamic pressures of up to 30 N m^{-2} on average, and up to a maximum of 120 N m^{-2}. By blending dynamic pressure maps with the extracted pixels of the tree-line ecotone, clear differences in dynamic pressure stress can be seen (Fig. 7). Mean dy-

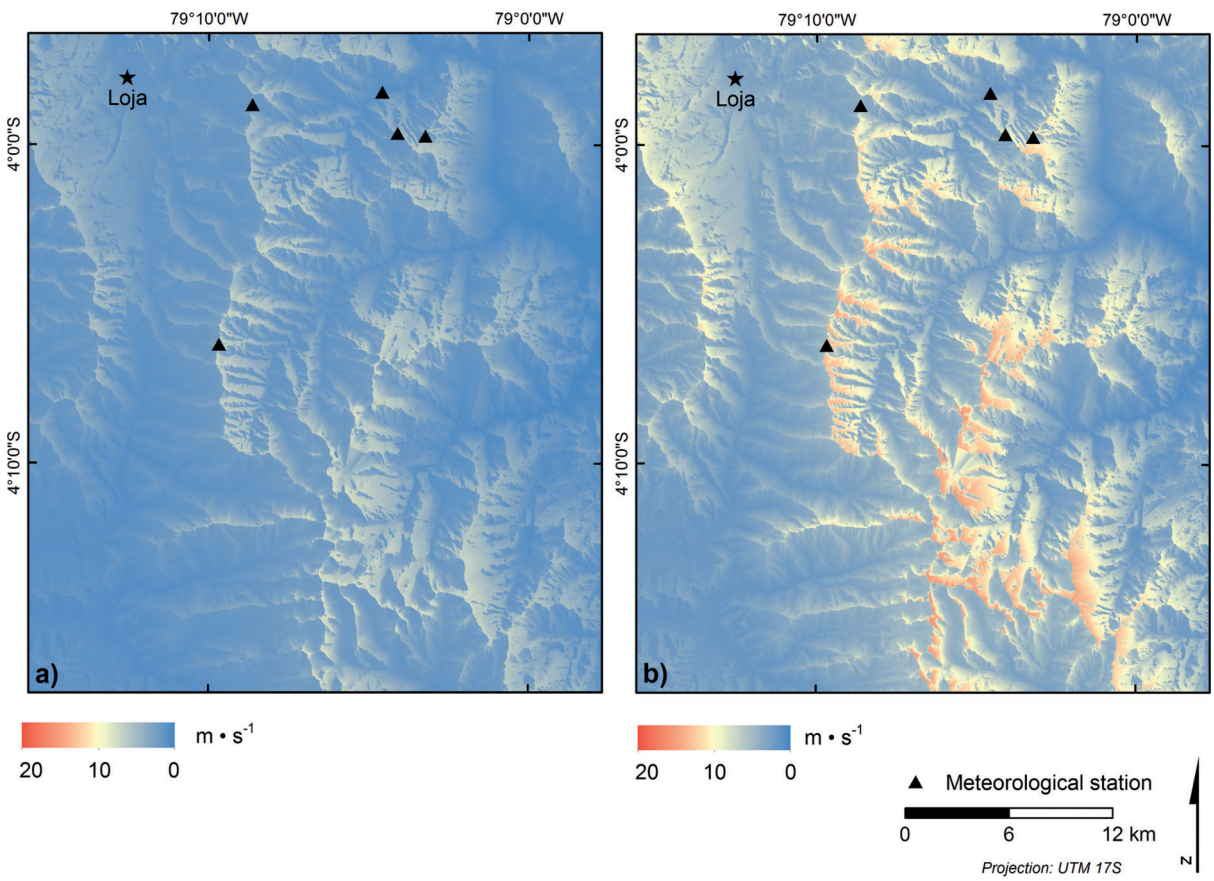

Fig. 5: Regionalized mean (a) and maximum (b) wind-speed maps in m s^{-1}

Tab. 4: Validation results for entire wind-speed maps

	Cerro, ECSF, El Tiro		Cerro, ECSF	
	Mean wind speed	**Maximum wind speed**	**Mean wind speed**	**Maximum wind speed**
p-value	0.01*	0.04*	0.00***	0.02*
Adj. R^2	0.27	0.16	0.76	0.38
RMSE	2.89	6.69	1.13	3.33

Note: Validation was done for a 3x3-pixel-window environment
Significance levels: 0 - ***, 0.001 - **, 0.01 - *, 0.05 -

namic pressures of up to 20 N m^{-2} occurred for the wind directions N, NE, E, SE and NW. In contrast, mean dynamic pressure values of up to 5 N m^{-2} predominated up to 90% of the time for the S, SW, W and NW directions. Higher dynamic pressure classes seldom occurred at these terrain exposures. The strongest mean dynamic pressure class rarely occurred. A similar pattern was found with the maximum dynamic pressures. The mid-level classes 40–60 N m^{-2} and 60–80 N m^{-2} accounted for a large proportion of winds for the NE and E directions. The low-level class 0–20 N m^{-2} strongly predominated in the S, SW and W directions, and other dynamic pressure classes are negligible. Dynamic pressures between 80 and 100 N m^{-2} occurred randomly in the N and NE directions. The high-level class 100–120 N m^{-2} occurred rarely. In summary, 90% of the tree-line ecotones facing S, SW and W were exposed to low-level mean and maximum dynamic pressures. For these wind directions the analysis results in a very homogenous pattern.

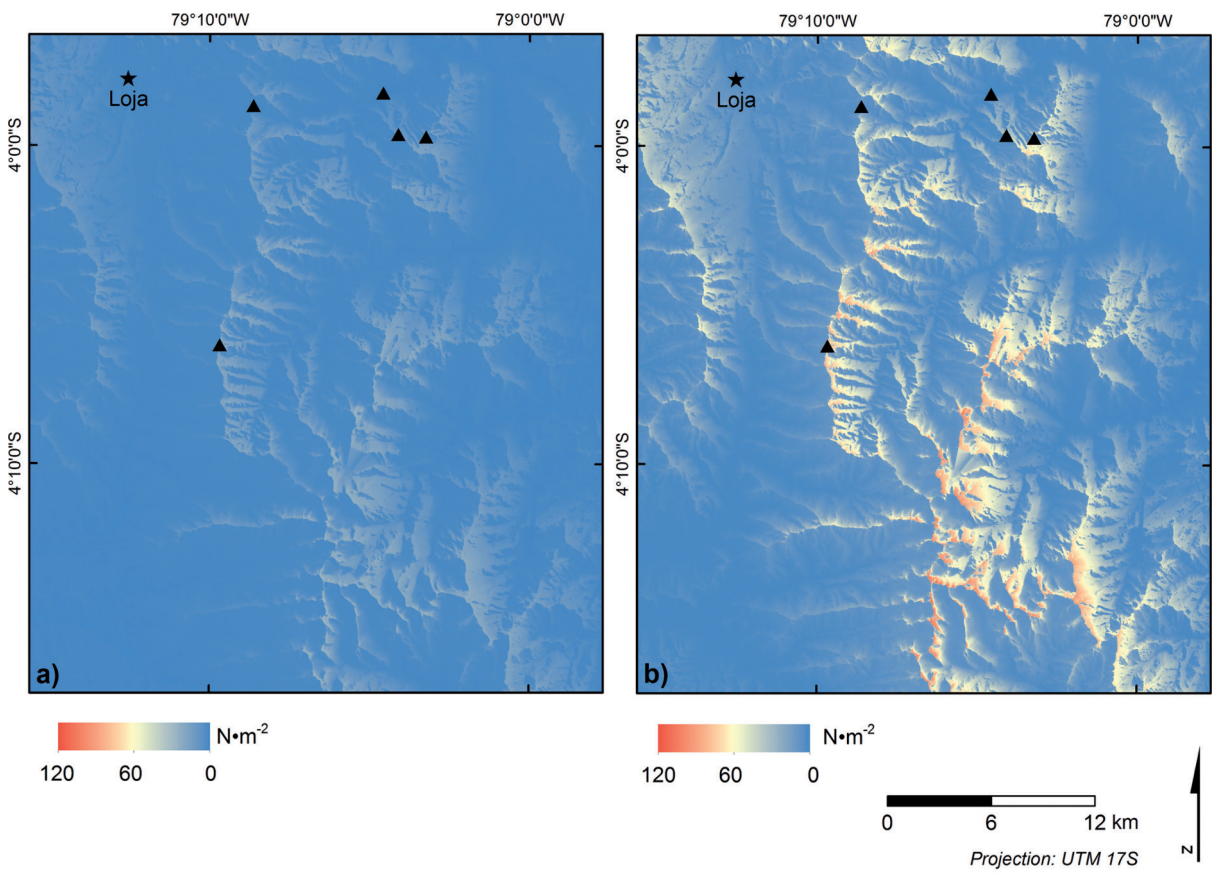

Fig. 6: Regionalized mean (a) and maximum (b) dynamic pressure maps in N m^{-2}

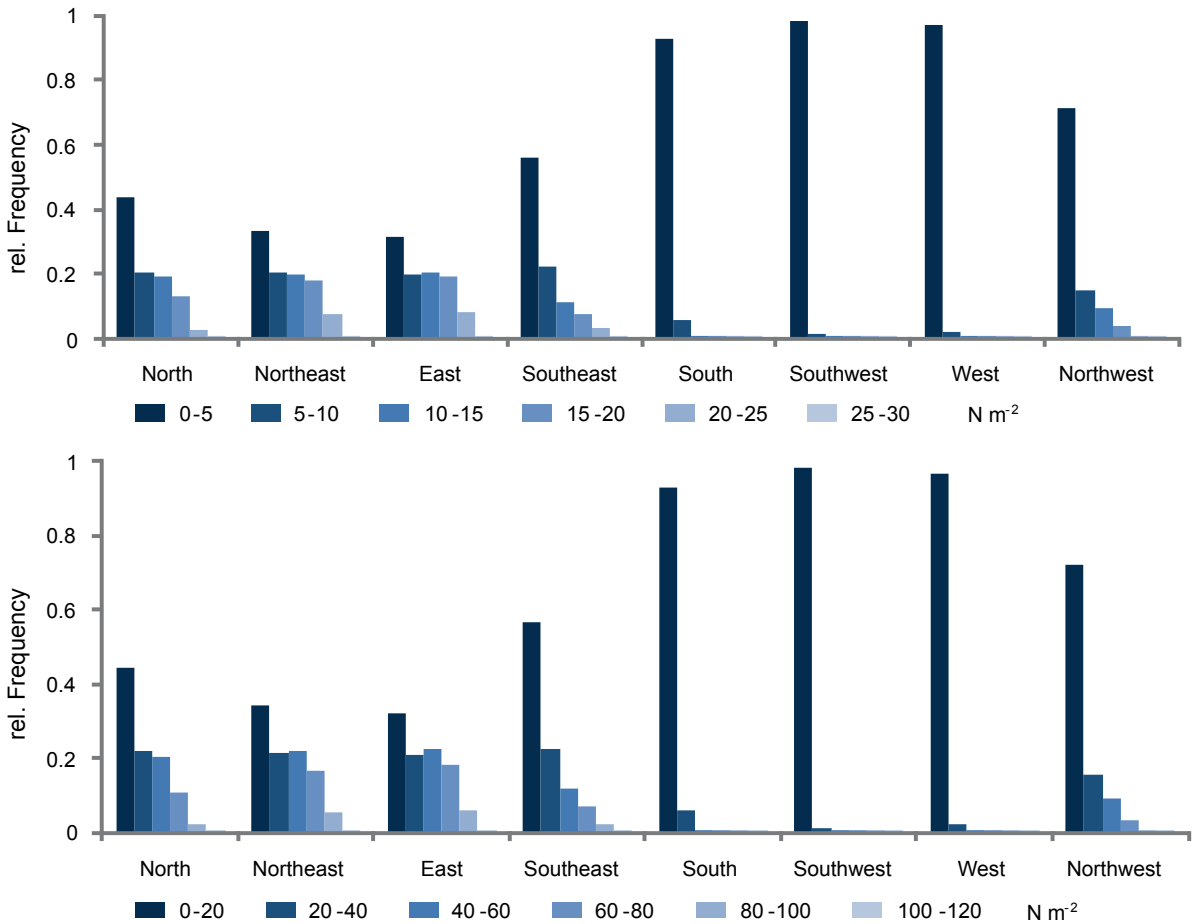

Fig. 7: Classification of the mean (a) and maximum (b) dynamic pressure classes for each terrain exposure along the tree-line ecotone

A more heterogeneous pattern appears for the tree-line ecotones facing NE and E: ~60% of the ecotones facing NE and ~61% of the ones facing E were exposed to mid- and high-level dynamic pressures. Altogether, tree-line ecotones facing E or NE were exposed to three to four times stronger dynamic pressure stress than the ones on the opposite side of the crest.

The question remains whether the higher wind pressure stress at the eastern slopes had an impact on the altitude of the tree line, as assumed by some studies mentioned in the introduction. The tree-line ecotone in the study area lies mainly between 2,800 to 3,400 m a.s.l. (Fig. 8, inset figure). This figure shows the mean difference of the average tree-line height on the eastern slopes (NE, E, SE) compared to westerly pixel expositions. Between 2,400 and 3,400 m a.s.l., a clear tendency towards lower altitudes can be detected for the eastern slopes of the Andes. On average, tree lines on exposed eastern ridges are ~50 m lower.

5 Discussion

The current study provides a promising approach to produce mean and maximum wind-speed and dynamic pressure maps for areas with complex topography and a sparse net of meteorological stations to assess the direct effects of wind exposure on the height of the tree-line ecotone. The approach uses meteorological point measurements and a digital elevation model to regionalize wind speeds. By applying the sheltering factor of Winstral and Marks (2002), altitudinal and topographic aspects were successfully considered. The validation gives considerable results, even if specific local phenomena such as acceleration caused by channelling effects (e.g. at El Tiro and partly at Cerro) cannot be captured accurately. The application of numerical non-hydrostatic mesoscale models like the widely used WRF (Weather Research and Forecasting model, Skamarock and Klemp 2008) might be a solu-

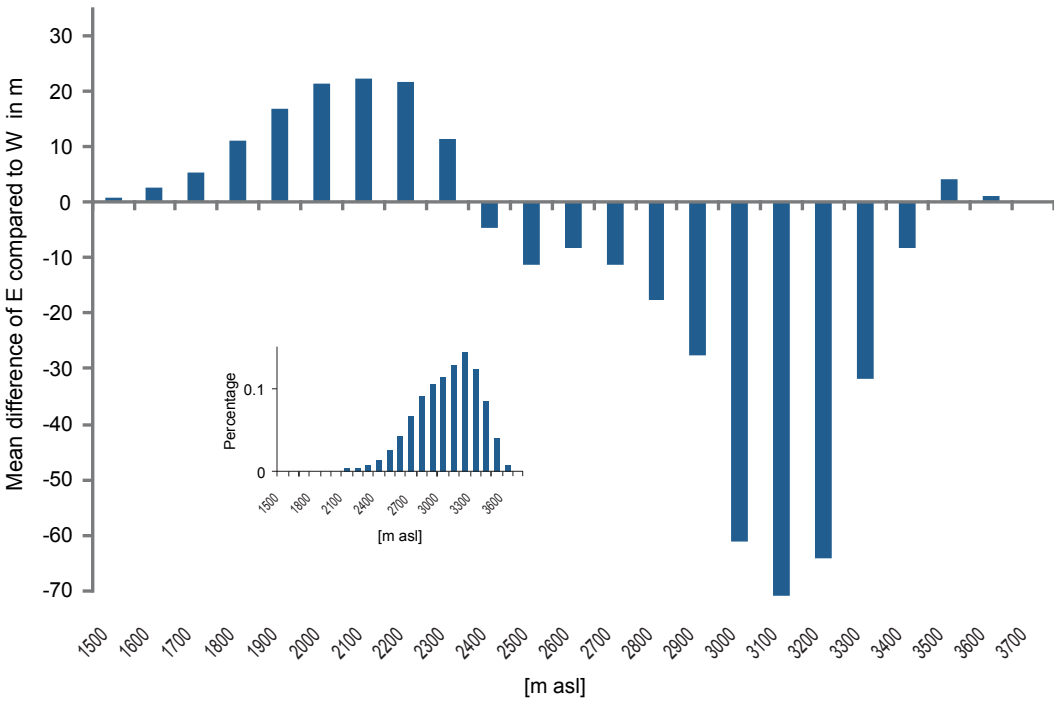

Fig. 8: Mean difference (east sector minus west sector) in m of the average height of the tree-line ecotone position for westerly (NW, W, SW) and easterly (NE, E, SE) pixel expositions. Frequencies are normalized regarding the number of tree-line pixels per wind sector (NE, E, SE: 1074693 pixels; NW, W, SW: 1047148 pixels). The inset shows the altitudinal distribution of the tree-line ecotone within the study area.

tion to minimize or even overcome such limitations. Butler et al. (2014) revealed on the basis of collected high-resolution surface wind-speed data in complex terrain that very high-resolution modelling (within the <100 m resolution) must be conducted in order to properly capture local wind components such as channelling effects and valley or slope breezes. However, these resolutions are mostly not provided by mesoscale model runs. Instead, some non-hydrostatic models specifically designed to calculate local breeze components depending e.g. on topography (as e.g. FITNAH "Flow over Irregional Terrain with Natural and Anthropogenic Heat Sources"; Gross 1991; Nielinger and Kost 2001; Gross 2002) should be applied. More detailed wind-speed and dynamic pressure maps considering local wind phenomena could result, at the cost of significantly higher efforts for local model adaptation and required computational power.

The ecological application of the mean and maximum dynamic pressure maps to investigate the influence of wind on the upper tree-line ecotone gives evidence of strong winds particularly resulting to a lowering of the tree-line ecotone of ~50 m. The question remains if and how different wind exposures might influence the tree-line position in the study area indirectly by modifying other microclimatic parameters (Bader and Ruijten 2008). On a global scale, Körner (1998; 2007) and Körner and Paulsen (2004) showed that growing season mean temperatures are the most important limiting factor for tree growth at the upper tree-line ecotone. According to them, mean temperatures below 5.5 °C (measured 10 cm below ground surface) are decisive for tree growth in the tropics. At the study sites, mean soil temperatures vary from 10.5 °C at Páramo to 11.4 °C at Cerro de Consuelo and cannot be considered as a cause for the lower tree line (Peters 2009; Bendix et al. 2010). Extraordinary incidence of solar radiation might favour the depression of the local tree-line ecotone (Peters 2009). Indeed, measurements demonstrate extraordinarily high radiation values at the upper tree-line ecotone in southern Ecuador. Especially during the dry phase from September to October, solar radiation is remarkably high, and values up to 1,832 W m^{-2} were recorded at the Páramo climate station (3,400 m a.s.l.; March 2000) (Emck 2008; Emck and Richter 2008). Field experiments by Bader et al. (2007) demonstrate that tree-seedling survival was highest in artificially shaded plots and under the forest canopy at the tree-line ecotone in northern Ecuador. This shelter ef-

fect was also proven in the study area to support the survival of saplings of indigenous tree species (Günter et al. 2009).

However, radiation is significantly reduced by clouds, particularly in the rainy season, also reducing photosynthesis (e.g. Silva et al. 2012). Cloudiness is patchy in the area and strongly elevated on wind-exposed slopes (Bendix et al. 2006). Particularly the higher altitudes of the eastern slopes with a lower tree-line ecotone experience high cloudiness and hence reduced radiation.

Thus, high amounts of rainfall and consequently higher environmental humidity might be an important indirect factor contributing to the lower tree line. Actually, spatial rain radar data and fog-water measurements show that the eastern windward slopes at crest altitudes have extraordinarily high amounts of rainfall and occult precipitation (Rollenbeck and Bendix 2011; Rollenbeck et al. 2011). This frequently results in waterlogging of soils (Bendix et al. 2013), leaching of nutrients (e.g. Bücker et al. 2011) and higher soil acidity and aluminium toxicity that inhibit tree growth (Richter et al. 2008; Peters 2009; Homeier et al. 2009), affecting the reproduction of indigenous tree species (Günter et al. 2009).

In summary, the direct effects of wind pressure and high humidity seem to be responsible for the lower tree lines in southern Ecuador. Fire, a potential human influence, may be excluded due to the extremely wet and windy conditions in the upper parts of the area. This is supported by change-detection analysis, which showed that the lower parts of the study area, far from the tree-line ecotone, are affected by human-induced forest destruction and fragmentation (Bendix 2013; Thies et al. 2014). It should be stressed that a lower tree line on windward slopes can be also observed in other areas of the Andes. On the windward side of a pristine mountain forest in the Venezuelan Andes Cuello et al. (2009) found it was about 100 m lower. This reduced altitude was explained as a combined effect of wind exposure, lower temperatures and higher rainfall. Duivenvoorden et al. (2012) discussed for this area that seed dispersal by animals and thus the reproduction of tree species might be facilitated by strong wind shelter. Other authors highlight the importance of rain-shadow effects in raising the Andean tree line (Young and Leon 2007). There, precipitation is significantly lower on the leeward side of the mountain ridge, resulting in reduced humidity and favouring conditions for tree establishment.

6 Conclusion

This study focused primarily on the influence of direct wind-pressure stress on a tropical tree-line ecotone in southern Ecuador. It is concluded that the vegetation structures were altered mainly by direct wind-pressure stress and to a smaller degree by secondary effects related to the high humidity. Future work should focus on more detailed analyses of these secondary wind effects on tree growth and the position of the tree-line ecotone. Therefore a thorough GIS model incorporating wind-pressure maps, rain, solar radiation, soil maps, etc. should be implemented.

Acknowledgements

The current study was conducted within the framework of the DFG Research Group FOR816 "Biodiversity and sustainable management of a megadiverse mountain rain forest in south Ecuador" and was generously funded by the German Research Foundation DFG (BE1780/15-2). Special thanks go to NCI (Loja) for logistic support, and the Ministry of the Environment of Ecuador (MAE) for the permission of the research.

References

Aulitzky, H. (1961): Die Bodentemperaturverhältnisse an einer zentralalpinen Hanglage beiderseits der Waldgrenze. I. Teil: Die Bodentemperatur oberhalb der zentralalpinen Waldgrenze. In: Arch. Met. Geoph. Biokl. B10, 445–532.

– (1962a): Die Bodentemperaturverhältnisse an einer zentralalpinen Hanglage beiderseits der Waldgrenze. II. Teil: Über die Bodentemperaturen im subalpinen Zirben-Lärchenwald. In: Arch. Met. Geophys. Biokl. B11, 301–362. DOI: 10.1007/Buff

– (1962b): Die Bodentemperaturverhältnisse an einer zentralalpinen Hanglage beiderseits der Waldgrenze. III. Teil: Die Bodentemperatur in ihren Beziehungen zu andern Klimafaktoren. In: Arch. Met. Geophys. Biokl. B11, 363–376. DOI: 10.1007/BF02244639

Bader, M. Y. and Ruijten, J. (2008): A topography-based model of forest distribution at alpine tree line in the tropical Andes. In: Journal of Biogeography 35, 711–723. DOI: 10.1111/j.1365-2699.2007.01818.x

Bader, M. Y.; Rietkerk, M. and Bregt, A. K. (2007): Vegetation structure and temperature regimes of tropical alpine tree lines. In: Arctic, Antarctic, and Alpine Research 39, 353–364. DOI: 10.1657/1523-0430(06-055)[BADER]2.0.CO;2

Beck, E.; Makeschin, F.; Haubrich, F.; Richter, M.; Bendix, J. and Valerezo, C. (2008): The ecosystem (Reserva Biológica San Francisco). In: Beck, E.; Bendix, J.; Kottke, I.; Makeschin, F. and Mosandl, R. (eds.): Gradients in a tropical mountain ecosystem of Ecuador. Berlin, Heidelberg, 1–13. DOI: 10.1007/978-3-540-73526-7_1

Bendix, J. (2004): Geländeklimatologie. Berlin, Stuttgart.

Bendix, J. (2013): Landnutzungsänderungen im Bereich des tropischen Bergregenwaldes Südecuadors. In: Bayerische Akademie der Wissenschaften: Rundgespräche der Kommission für Ökologie 42, 75–84.

Bendix, J. and Beck, E. (2009): Spatial aspects of ecosystem research in a biodiversity hot spot of southern Ecuador - an introduction. In: Erdkunde 63, 305–308. DOI: 10.3112/erdkunde.2009.04.01

Bendix, J. and Rafiqpoor, M. D. (2001): Studies on the thermal conditions of soils at the upper tree line in the Páramo of Papallacta (Eastern Cordillera of Ecuador). In: Erdkunde 55, 257–276. DOI: 10.3112/erdkunde.2001.03.04

Bendix, J.; Rollenbeck, R.; Göttlicher, D. and Cermak, J. (2006): Cloud occurrence and cloud properties in Ecuador. In: Climate Research 30, 133–147. DOI: 10.3354/cr030133

Bendix, J.; Rollenbeck, R.; Richter, M.; Fabian, P. and Emck, P. (2008): Climate. In: Beck, E.; Bendix, J.; Kottke, I.; Makeschin, F. and Mosandl, R. (eds.): Gradients in a tropical mountain ecosystem of Ecuador. Berlin, Heidelberg, 63–74. DOI: 10.1007/978-3-540-73526-7_8

Bendix, J.; Trachte, K.; Cermak, J.; Rollenbeck, R. and Nauss, T. (2009): Formation of convective clouds at the foothills of the tropical eastern Andes (South Ecuador). In: Journal of Applied Meteorology and Climatology 48, 1682–1695. DOI: 10.1175/2009JAMC2078.1

Bendix, J.; Behling, H.; Peters, T.; Richter, M. and Beck, E. (2010): Functional biodiversity and climate change along an altitudinal gradient in a tropical mountain rainforest. In: Tscharnke, T.; Leuschner, C.; Veldkamp, E.; Faust, H.; Guhardja. E. and Bidin, A. (eds.): Tropical rainforests and agroforests under global change. Berlin, Heidelberg, 293–308. DOI: 10.1007/978-3-642-00493-3_11

Bendix, J.; Dislich, C.; Huth, A.; Huwe, B.; Ließ, M.; Schröder, B.; Thies, B.; Vorpahl, P.; Wagemann, J. and Wilcke, W. (2013): Natural landslides which impact current regulating services: environmental preconditions and modelling. In: Ecological Studies 221, 153–170. DOI: 10.1007/978-3-642-38137-9_12

Bücker, A.; Crespo, P.; Frede, H. and Breuer, L. (2011): Solute behaviour and export rates in neotropical montane catchments under different land-uses. In: Journal of Tropical Ecology 27, 305–317. DOI: 10.1017/S0266467410000787

Butler, B. W.; Wagenbrenner, N. S.; Forthofer, J. M.; Lamb, B. K.; Shannon, K. S.; Finn, D.; Eckman, R. M.; Clawson, K.; Bradshaw, L.; Sopko, P.; Beard, S.; Jimenez, D.; Wold, C. and Vosburgh, M. (2014): High resolution observations of the near-surface wind field over an isolated mountain and in a steep river canyon. In: Atmospheric Chemistry and Physics Discussion 14, 16821–16863. DOI: 10.5194/acpd-14-16821-2014

Cuello, A.; Nidia, L. and Cleef, A. M. (2009): The forest vegetation of Ramal de Guaramacal in the Venezuelan Andes. In: Phytocoenologia 39, 109–156. DOI: 10.1127/0340-269X/2009/0039-0109

Duivenvoorden, J. F.; Nidia, L. A. and Cuello, A. (2012): Functional trait state diversity of Andean forests in Venezuela changes with altitude. In: Journal of Vegetation Science 23, 1105–1113. DOI: 10.1111/j.1654-1103.2012.01428.x

Emck, P. (2008): A climatology of South Ecuador: with special focus on the major Andean climate divide. Saarbrücken.

Emck, P. and Richter, M. (2008): An upper threshold of enhanced global shortwave irradiance in the troposphere derived from field measurements in tropical mountains. In: Journal of Applied Meteorology and Climatology 47, 2828–2845. DOI: 10.1175/2008JAMC1861.1

Etienne, C.; Lehmann, A. and Goyette, S. (2010): Spatial predications of extreme wind speeds over Switzerland using generalized additive models. In: Journal of Applied Meteorology and Climatology 49, 1956–1970. DOI: 10.1175/2010JAMC2206.1

Fries, A.; Rollenbeck, R.; Nauss, T.; Peters, T. and Bendix, J. (2012): Near surface air humidity in a megadiverse Andean mountain ecosystem of southern Ecuador and its regionalization. In: Agricultural and Forest Meteorology 152, 17–30. DOI: 10.1016/j.agrformet.2011.08.004

Göttlicher, D.; Obregón, A.; Homeier, J.; Rollenbeck, R.; Nauss, T. and Bendix, J. (2009): Land cover classification in the Andes of southern Ecuador using Landsat ETM+ data as a basis for SVAT modeling. In: International Journal of Remote Sensing 30, 1867–1886. DOI: 10.1080/01431160802541531

Gross, G. (1991): Das dreidimensionale, nichthydrostatische Mesoscale-Modell FITNAH. In: Meteorologische Rundschau 43, 97–112.

– (2002): The exploration of boundary layer phenomena using a nonhydrostatic mesoscale model. In: Meteorologische Zeitschrift 11, 295–302. DOI: 10.1127/0941-2948/2002/0011-0295

Günter, S.; González, P.; Alvarez, G.; Aguirre, N.; Palomeque, X.; Haubrich, F. and Weber, M. (2009): Determinants for successful reforestation of abandoned pastures in the Andes: soil conditions and vegetation cover. In: Forest Ecology and Management 258, 81–91. DOI: 10.1016/j.foreco.2009.03.042

Holtmeier, F.-K. (2009): Mountain timberlines. Ecology, patchiness, and dynamics. Dordrecht.

Holtmeier, F.-K. and Broll, G. (2010): Wind as an ecological agent at tree lines in North America, the Alps, and the European subarctic. In: Physical Geography 31, 203–233. DOI: 10.2747/0272-3646.31.3.203

Homeier, J.; Werner, F. A.; Gradstein, S. R.; Breckle, S.-W. and Richter, M. (2008): Potential vegetation and floristic composition of Andean forests in South Ecuador, with a focus on the RBSF. In: Beck, E.; Bendix, J.; Kottke, I.; Makeschin, F. and Mosandl, R. (eds.): Gradients in a tropical mountain ecosystem of Ecuador. Berlin, Heidelberg, 87–100. DOI: 10.1007/978-3-540-73526-7_10

Homeier, J.; Breckle, S. W.; Günter, S.; Rollenbeck, R. and Leuschner, C. (2009): Tree diversity, forest structure and productivity along altitudinal and topographical gradients in a species-rich Ecuadorian montane rainforest. In: Biotropica 42 (2), 140–148. DOI: 10.1111/j.1744-7429.2009.00547.x

Jordan, E.; Ungerechts, L.; Cáceres, B. and Penafiel, A. (2005): Estimation by photogrammetry of the glacier recession on the Cotopaxi Volcano (Ecuador) between 1956 and 1997. In: Hydrological Sciences Journal 50, 949–961. DOI: 10.1623/hysj.2005.50.6.949

Körner, C. (1998): A re-assessment of high elevation tree line positions and their explanation. In: Oecologia 115, 445–459. DOI: 10.1007/s004420050540

– (2007): Climatic treelines: conventions, global patterns, causes. In: Erdkunde 61, 316-324. DOI: 10.3112/erdkunde.2007.04.02

Körner, C. and Paulsen, J. (2004): A world-wide study of high altitude tree line temperatures. In: Journal of Biogeography 31, 713–732. DOI: 10.1111/j.1365-2699.2003.01043.x

Lun, I. Y. F. and Lam, J. C. (2000): A study of Weibull parameters using long-term wind observations. In: Renewable Energy 20, 145–153. DOI: 10.1016/S0960-1481(99)00103-2

Luo, W.; Taylor, M. C. and Parker, S. R. (2008): A comparison of spatial interpolation methods to estimate continuous wind speed surfaces using irregularly distributed data from England and Wales. In: International Journal of Climatology 28 (7), 947–959. DOI: 10.1002/joc.1583

Malanson, G. P.; Resler, L. M.; Bader, M. Y.; Holtmeier, F.-K.; Butler, D. R.; Weiss, D. J.; Daniels, L. D. and Fagre, D. B. (2011): Mountain tree lines: a roadmap for research orientation. In: Arctic, Antarctic and Alpine Research 43 (2), 167–177. DOI: 10.1657/1938-4246-43.2.167

Nielinger, J. and Kost, W. J. (2001): Simulation of realistic location-related wind distributions with the mesoscale model FITNAH. In: Meteorologische Zeitschrift 10, 235–238. DOI: 10.1127/0941-2948/2001/0010-0235

Palomino, I. and Martin, F. (1994): A simple method for spatial interpolation of the wind in complex terrain. In: Journal of Applied Meteorology 34, 1678–1692. DOI: 10.1175/1520-0450-34.7.1678

Pennypacker S. P.; Knoble H. D.; Antle C. E. and Madden L. V. (1980): A flexible model for studying plant disease progression. In: Phytopatology 70, 232–235. DOI: 10.1094/Phyto-70-232

Peters, T. (2009): Struktur und ökologische Merkmale der oberen Waldgrenze in der Andinen Depression. PhD thesis. Erlangen.

Richter, M.; Diertl, K.-H.; Peters, T. and Bussmann, R. W. (2008): Vegetation structures and ecological features of the upper timberbline. In: Beck, E.; Bendix, J.; Kottke, I.; Makeschin, F. and Mosandl, R. (eds.): Gradients in a tropical mountain ecosystem of Ecuador. Berlin, Heidelberg, 123–135. DOI: 10.1007/978-3-540-73526-7_13

Rinne, H. (2009[2]): The Weibull distribution: a handbook. Boca Raton.

Rollenbeck, R. and Bendix, J. (2011): Rainfall distribution in the Andes of southern Ecuador derived from blending weather radar data and meteorological field observations. In: Atmospheric Research 99, 277–289. DOI: 10.1016/j.atmosres.2010.10.018

Rollenbeck, R.; Bendix, J. and Fabian, P. (2011): Spatial and temporal dynamics of atmospheric water inputs in tropical mountain forests of South Ecuador. In: Hydrological Processes 25, 344–352. DOI: 10.1002/hyp.7799

Ryan, B. C. (1977): A mathematical model for diagnosis and prediction of surface winds in mountainous terrain. In: Journal of Applied Meteorology 16 (6), 571–584. DOI: _10.1175/1520-0450(1977)016<0571:AMMFDA>2.0.CO;2

Silva, B.; Roos, K.; Voss, I.; König, N.; Rollenbeck, R.; Scheibe, R.; Beck, E. and Bendix, J. (2012): Simulating canopy photosynthesis for two competing species of an anthropogenic grassland community in the Andes of southern Ecuador. In: Ecological Modelling 239, 14–26. DOI: 10.1016/j.ecolmodel.2012.01.016

Skamarock, W. C. and Klemp, J. B. (2008): A time-split nonhydrostatic atmospheric model for weather research and forecasting applications. In: Journal of Computational Physics 227, 3465–3485. DOI: 10.1016/j.jcp.2007.01.037

Trachte, K.; Nauss, T. and Bendix, J. (2010): The impact of different terrain configurations on the formation and dynamics of katabatic flows: idealised case studies. In: Boundary-Layer Meteorology 134, 307–325. DOI: 10.1007/s10546-009-9445-8

Thies, B.; Meyer, H.; Nauss, T. and Bendix, J. (2014): Projecting land use and land cover changes in a tropical mountain forest of southern Ecuador. In: Journal of Land Use Science 9, 131–131. DOI: 10.1080/1747423X.2012.736197

Turner, H. (1971): Mikroklimatographie und ihre Anwendung in der Ökologie der subalpinen Stufe. In: Annalen der Meteorologie N.F. 5, 275–281.

Weisser, D. (2003): A wind energy analysis of Grenada: an estimation using the Weibull density function. In: Renewable Energy 28, 1803–1812. DOI: 10.1016/S0960-1481(03)00016-8

Wilks, D. S. (2008[3]): Statistical methods in the atmospheric sciences. Heidelberg.

Winstral, A. and Marks, D. (2002): Simulating wind fields and snow redistribution using terrain-based parameters to model snow accumulation and melt over a semi-arid mountain catchment. In: Hydrological Processes 16, 3585–3603. DOI: 10.1002/hyp.1238

Wörlen, C.; Schulz, K.; Huwe, B. and Eiden, R. (1999): Spatial extrapolation of agrometeorological variables. In: Agricultural and Forest Meteorology 94, 233–242. DOI: 10.1016/S0168-1923(99)00015-5

Xia, Y.; Fabian, P.; Winterhalter, M. and Zhao, M. (2000): Forest climatology: estimation and use of daily climatological data for Bavaria, Germany. In: Agricultural and Forest Meteorology 106, 87–103. DOI: 10.1016/S0168-1923(00)00210-0

Young, K. R. and Leon, B. (2007): Tree-line changes along the Andes: implications of spatial patterns and dynamics. In: Philosophical Transactions of the Royal Society B362, 263–272. DOI: 10.1098/rstb.2006.1986

Yoshimura, M. (1971): Die Windverbreitung im Gebiet des Mt. Fuji. In: Erdkunde 25 (3), 195–198. DOI: 10.3112/erdkunde.1971.03.03

Authors

Julia Wagemann
ESA/ESRIN
Via Galileo Galilei
Casella Postale 64
IT-00044 Frascati
Italy
wagemann.julia@gmx.de

Dr. Boris Thies,
PD Dr.Rütger Rollenbeck
Prof Dr. Jörg Bendix
Laboratory for Climatology and
Remote Sensing (LCRS)
Faculty of Geography
University of Marburg
Deutschhausstraße 10
D-35032 Marburg
Germany
thies@staff.uni-marburg.de
rollenb@staff.uni-marburg.de
bendix@staff.uni-marburg.de

Dr. Thorsten Peters
Institute of Geography
University of Erlangen-Nuremberg
Wetterkreuz 15
D-91058 Erlangen
Germany
thorsten.peters@fau.de